Journal of Luminescence 222 (2020) 117172

Contents lists available at ScienceDirect

Journal of Luminescence

journal homepage: http://www.elsevier.com/locate/jlumin

Spatial anomalies in spectral-kinetic properties of Pr^{3+} - Doped $LiY_{1-x}Lu_xF_4$ mixed crystals☆

V.G. Gorieva [a,**], A.A. Lyapin [b], S.L. Korableva [a], P.A. Ryabochkina [b], V.V. Semashko [a]

[a] Institute of Physics, Kazan Federal University, Kremlevskaya Street 18, Kazan, 420008, Russia
[b] Institute of Physics and Chemistry, National Research Mordovia State University, Bol'shevitskaya Street 68, Saransk, 430005, Russia

ARTICLE INFO

Keywords:
Rare earth doped materials
Solid state lasers
Visible lasers
Spectroscopy
Excited-state absorption
Fluoride crystals

ABSTRACT

We present the spectral-kinetic including excited state absorption spatial-dependent features of Pr^{3+} - doped $LiY_{1-x}Lu_xF_4$ mixed crystals grown by Bridgeman technique.

1. Introduction

The praseodymium doped dielectric crystals and glasses are very attractive for design of visible lasers based on 4f-4f transitions of praseodymium ions and for UV lasing performed by subsequent conversion to the second harmonic. The visible laser action was realized in several crystal hosts and glasses doped with Pr^{3+} ions: $LiYF_4$, $LiLuF_4$, $LiY_{0.3}Lu_{0.7}F_4$ $LiGdF_4$, KYF_4, KY_3F_{10}, LaF_3, BaY_2F_8, $YAlO_3$, $SrAl_{12}O_{19}$, ZBLAN and ZBLA [1–5]; the UV and near-UV lasing was demonstrated by the visible laser operation intracavity frequency doubling at 261 [6], 302 [7], 303 [8], 320 [2,9–11], 349 [12] and 360 nm [13] in Pr:$LiYF_4$, 303.5 nm in Pr:BaY_2F_8 [14], 305 nm in Pr:KY_3F_{10} [15], 284 nm using both Pr: YLF and Nd: YVO_4 [16], 373.5 nm in Pr:$YAlO_3$ [17,18], 320 nm in Pr: $LiLuF_4$ [10], 320 nm in Pr:BaY_2F_8 [11]. The most of the publications are devoted to $LiYF_4$ and $LiLuF_4$ hosts providing the best and the variable laser properties.

The prospect of visible and UV lasers development is obvious because they can be used in the several regions of human needs. Only applications in such important areas as medicine and biology are impressive: in ophthalmology for treatment of vascular diseases and retina; in dermatology for treatment of allergic dermatitis, psoriasis, pyoderma, vasculitis, scleroderma, viral dermatitis, vitiligo, angiokeratomas, telangiectasia, poikiloderma of Civatte etc.; in cosmetology for hair and tattoo removal, not ablative resurfacing, removal of benign pigmented lesions, etc.; for intravenous laser blood irradiation (ILBI); in stomatology for caries detection; in surgery; in cardiology for atherosclerotic plaques removal; in biology for matrix-assisted laser desorption ionization–time of flight mass spectrometry, thermal sensing of a single eukaryotic cell internalized with nanoparticles, antimicrobial photodynamic therapy, bacterial identification and many others [19–23].

It is well known that the key parameters determining the opportunity of effective laser action and the intracavity second harmonic generation are: the cross-sections of absorption spectra from the ground and excited states (GSA and ESA, correspondently) and stimulated emission, fluorescence kinetics and quantum yield properties, distribution coefficient of the dopant, the optical quality of the crystal etc. In practice, the essential role of the choice of the crystal matrix is the cost of the host chemical compounds and the technological expenses for the unit of crystalline active element. To reach a balance between distribution coefficient of light rare earth elements that higher for $LiYF_4$ host, cost of chemical components that lower for $LiYF_4$ host, technological advantages and optical quality that higher for $LiLuF_4$ and associated with the congruent melting character of the one [24–27], the solid solution of $LiY_{1-x}Lu_xF_4$ with the variable parameter « x » can be used. These mixtures were also studied as perspective UV laser materials [28].

In the present search we studied the series of the crystals Pr^{3+}:$LiY_{1-x}Lu_xF_4$ with the varied x-parameter form 0 to 1. Moreover the spectral-kinetic features of the samples were studied along the crystal boules. It

☆ Declarations of interest: none.

* Corresponding author.
E-mail addresses: vgorieva@gmail.com (V.G. Gorieva), andrei_lyapin@mail.ru (A.A. Lyapin), safkorstella@mail.ru (S.L. Korableva), ryabochkina@mail.ru (P.A. Ryabochkina), ua4pcy@mail.ru (V.V. Semashko).

https://doi.org/10.1016/j.jlumin.2020.117172
Received 20 August 2019; Received in revised form 26 February 2020; Accepted 27 February 2020
Available online 29 February 2020

was done because we revealed the mismatches in published Pr:$LiYF_4$ and Pr:$LiLuF_4$ ground state absorption (GSA) $^3H_4 \rightarrow {}^3P_j$ spectra studied by different research groups [29–36] and the changing of the appropriate line intensities along Pr:$LiY_{0.3}Lu_{0.7}F_4$ and Pr:$LiYF_4$ crystal boules [37]. Also $^3P_0$ manifold lifetime measurements of [10] discovered concentration dependence for Pr:$LiYF_4$ samples. To reveal any anomaly of GSA, ESA, luminescence spectra and in the kinetics of $^3P_0$–$^3H_4$ luminescence of the Pr^{3+} ions we studied the ones in several points along the crystal growth direction for the seven fluoride crystals 1 at% Pr:$LiY_{1-x}Lu_xF_4$ (x = 0, 0.3, 0.5, 0.6, 0.7, 0.8, 1) and low-concentrated 0.1 at% Pr:$LiY_{0.3}Lu_{0.7}F_4$ sample.

2. Samples

Seven fluoride crystals Pr:$LiY_{1-x}Lu_xF_4$ (x = 0, 0.3, 0.5, 0.6, 0.7, 0.8, 1) were grown by Bridgeman technique in carbon crucible under Ar-gas overpressure. The crystal-pulling rate was 1.5 mm/h. The dopant concentration in the melt was 1 at% and was the same for all the samples. The grown bulks had a shape of the truncated cone with the 5.4 mm diameter at the beginning of growth and about 6 mm at the end of the one. The length of the crystals was about 30 mm. Two parallel plane windows were polished along the growth direction for all the crystals (Fig. 1). The optical axis *c* is situated in the plane of their surfaces. The thickness of the samples between these windows was 5 mm.

Three additional crystals 2 at% Tm:$LiYF_4$, 1 at% Er:$LiYF_4$ and low-concentrated 0.1 at% sample Pr:$LiY_{0.3}Lu_{0.7}F_4$ were also prepared as the reference samples to study any possible spatial anomaly in spectral-kinetics properties along the crystalline boules.

3. Spectral and kinetic measurements

Polarized absorption and luminescence spectra of Pr:$LiY_{1-x}Lu_xF_4$ (x = 0, 0.3, 0.5, 0.6, 0.7, 0.8, 1) samples were taken in 7–10 areas along bulk of the samples at room temperature. The areas were limited by 2 mm pinholes separated by 3 mm distance between each other (Fig. 2). Absorption spectra of the samples were studied by using Perkin–Elmer spectrophotometer Lambda 950 at 0.05 nm spectral resolution in the visible spectral range and 0.2 nm in infrared.

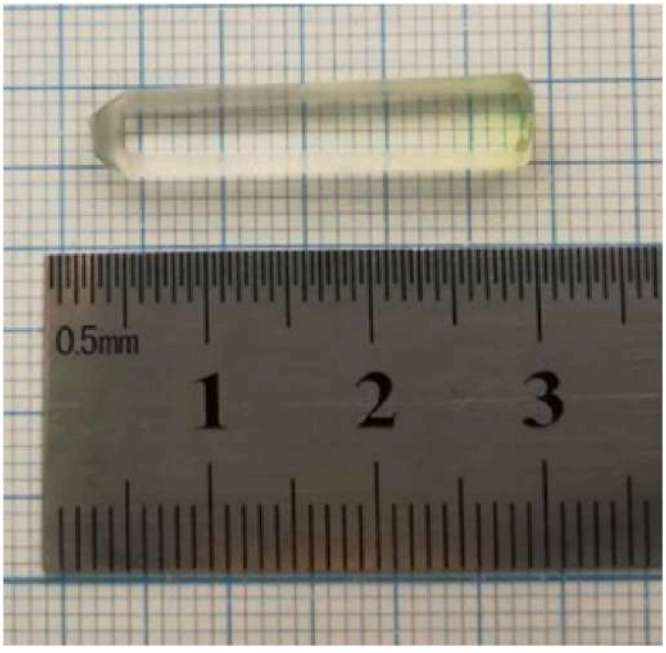

Fig. 1. One of the typical samples of Pr:$LiY_{1-x}Lu_xF_4$ crystals using in the experiments.

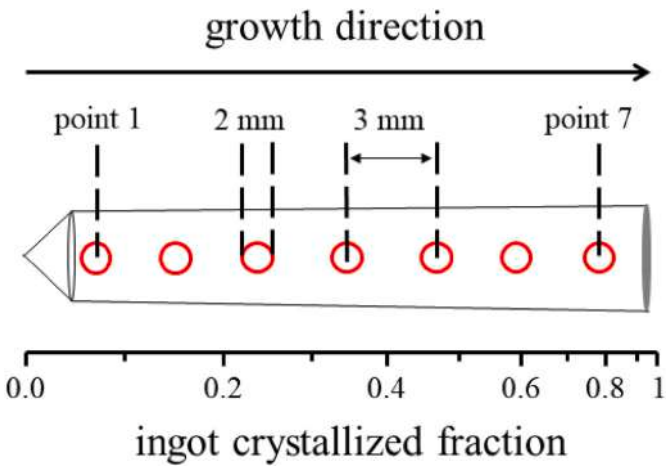

Fig. 2. The scheme of arrangement of the studied areas along crystal bulk.

3.1. Absorption spectroscopy of Pr:$LiY_{1-x}Lu_xF_4$ crystals

Absorption spectra were recorded in 420–2400 nm region. The typical spectra in the beginning parts of the bulk (point or area number 1 or 2 on Fig. 2) are presented on Fig. 3.

Absorption spectra of the beginning, middle and end of the Pr:$LiY_{1-x}Lu_xF_4$ crystals for $^3H_4$-$^1D_2$,^3P_j are presented in Fig. 4 in details.

As it can be seen, there is the decreasing of $^3H_4 \rightarrow {}^3P_0$ absorption line intensity with respect to $^3H_4 \rightarrow {}^3P_2$ and $^3H_4 \rightarrow {}^3P_1$ lines depending on the distance from the sample's initial point of crystallization. This tendency is inherent for all 1% Pr:$LiY_{1-x}Lu_xF_4$ crystals for π-polarized spectra only whereas the shape of σ-polarized ones stays the same.

We estimated the ratios of integral intensities of $^3H_4$ – $^3P_0$ (479 nm), $^3P_1$ (469 nm), $^3P_2$ (443 nm), $^1D_2$ (595 nm), $^3F_2$ (1557 nm), $^3F_3$ (1910 nm) GSA bands [33,38] along crystal growth for π and σ polarizations. Results are partially presented on Fig. 5 versus the ingot crystallized part g and Pr^{3+} ions content. The Pr^{3+} ions concentrations along the crystal growth were calculated on the base of the distribution coefficients data of Pr^{3+} ions in $LiY_{1-x}Lu_xF_4$ crystals determined in our previous work [1].

All the ratios for the all samples stay the same except ones for π-polarized spectra associated with $^3H_4$ – $^3P_0$ transitions. The dependencies had a nonmonotonic character depending on ingot crystallized part g (Fig. 5 a, c, e): from the beginning to the middle of the crystal boules the weak tendency of the dropping of the ratios is observed

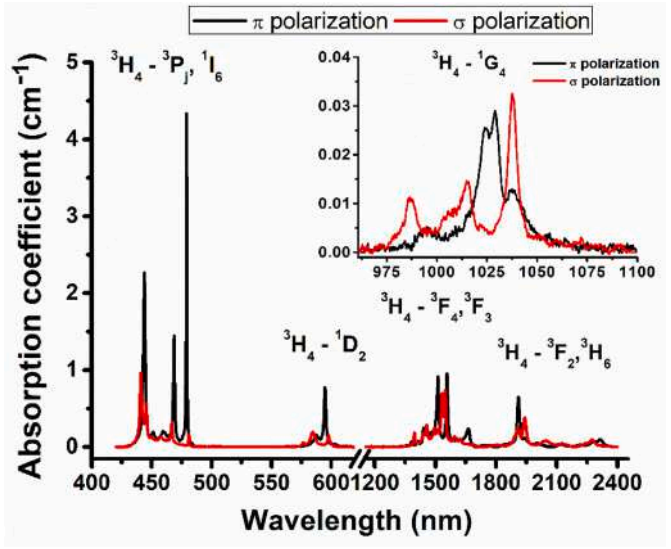

Fig. 3. The typical GSA spectra in the beginning parts of Pr:$LiY_{1-x}Lu_xF_4$ crystals.

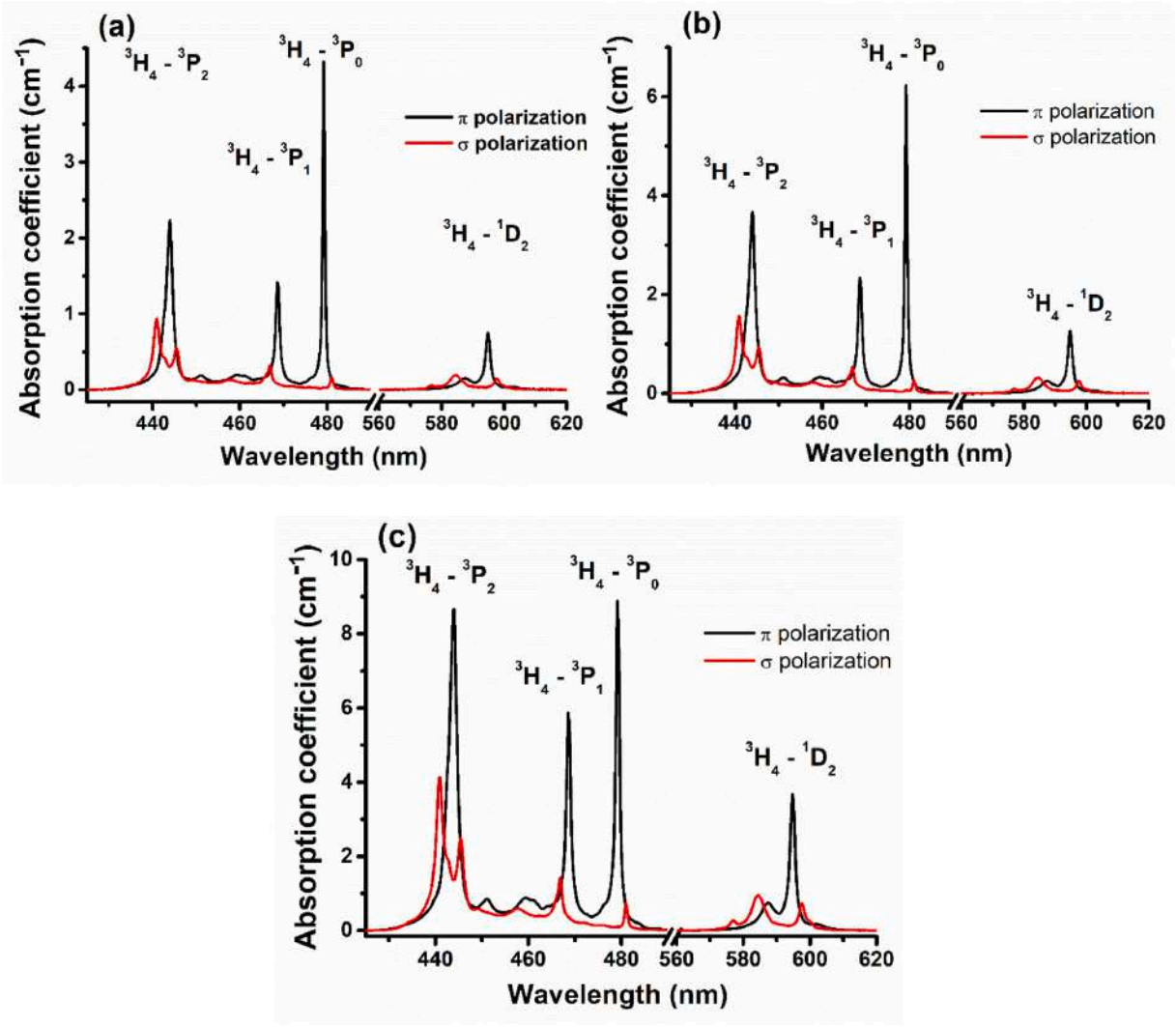

Fig. 4. The GSA spectra of the beginning (a), middle (b) and end (c) of the Pr:$LiY_{1-x}Lu_xF_4$ crystals.

whereas in the rest area of the samples it decreases faster. Following the results of [1] this behavior can be attributed to the growth of the Pr^{3+} ions content along the crystal boule (see Fig. 5 b, d, f). The typical dependences for other ratios are depicted on Fig. 5 (g, h, i, j).

It is surprising, but for hypersensitive transitions $^3H_4$–$^3P_2$ (Fig. 5 g and h) and $^3H_4$–$^3F_2$ (Fig. 5 i and j) [39,40] the similar dependences were not observed.

The ratios of integral absorption spectra for π- and σ-polarization associated with $^3H_4$-^3P_j and $^3H_4$-$^1D_2$ transitions for the all samples are depicted on Fig. 6. It can be seen the ratio for π-polarized spectra is also nonpermanent.

To elucidate the nature of such phenomena manifestations - growth conditions or concentration of the dopant – we studied Er:$LiYF_4$ and Tm:$LiYF_4$ crystals. In contrast to Pr^{3+} ions the distribution coefficient of Er^{3+} and Tm^{3+} in $LiYF_4$ is near to unity due to small differences between their and Y^{3+} ions radii. Hence their concentrations along crystal growth are almost constant. The absorption spectra were registered in 300–1200 nm range for Er:$LiYF_4$ and 300–1000 nm range for Tm:$LiYF_4$ crystals. No any spatial anomalies were observed for the spectra. So, we can make a conclusion that all the anomalies have precisely the concentration-related nature. Our assumption is confirmed by results of [41] where the authors revealed the similar concentration-related absorption spectra of Yb^{3+} in BaF_2 matrix. Increase of concentration of Pr^{3+} ions along crystal growth apparently leads to a change in the local environment of these ions that can be expressed in the formation of clusters. These experimental results require further detailed theoretical analysis.

Also the broadening of $^3H_4$-^3P_j absorption lines of Pr^{3+} ions and the absence of the one for $^3H_4$-$^1D_2$ transitions were revealed. As a relative parameter of broadening we present the dependences of the integral GSA spectra of Pr^{3+} to $^3P_0$ and $^3P_2$ manifolds normalized on its maxima (Fig. 7) as a function of concentration. The dependencies are close to linear.

3.2. *Luminescence measurements of Pr:$LiY_{1-x}Lu_xF_4$ crystals*

The luminescence excitation was provided by 3 ns (FWHM) pulses at 442.7 nm of OPO LT-2215PC (LOTIS) pumped by 3ω-radiation of Nd:YAG LS-2134UTF (LOTIS) at 10 Hz pulse repetition rate. The luminescence signal was separated by MDR-3 monochromator at 479.4 nm and the decays were registered by photomultiplier FEU-87 attached to Bordo 211A oscilloscope with a bandwidth of 200 MHz.

The polarized luminescence spectra from the ^3P_j state were registered in 300–1000 nm spectral range by Stellarnet spectrometer corrected for its spectral sensitivity (Fig. 8). The similar spatial anomalies were revealed - the $^3P_0$–$^3H_4$ luminescence intensity demonstrates decreasing for both polarizations as a function of ingot crystallized part and concentration of Pr^{3+} ions (Fig. 9) despite the fact that, for instance, $^3P_0$–$^3H_6$ luminescence intensity almost does not change. Stimulated emission cross-section is related to absorption cross-section through McCumber law [42]. So the effect of luminescence decreasing we

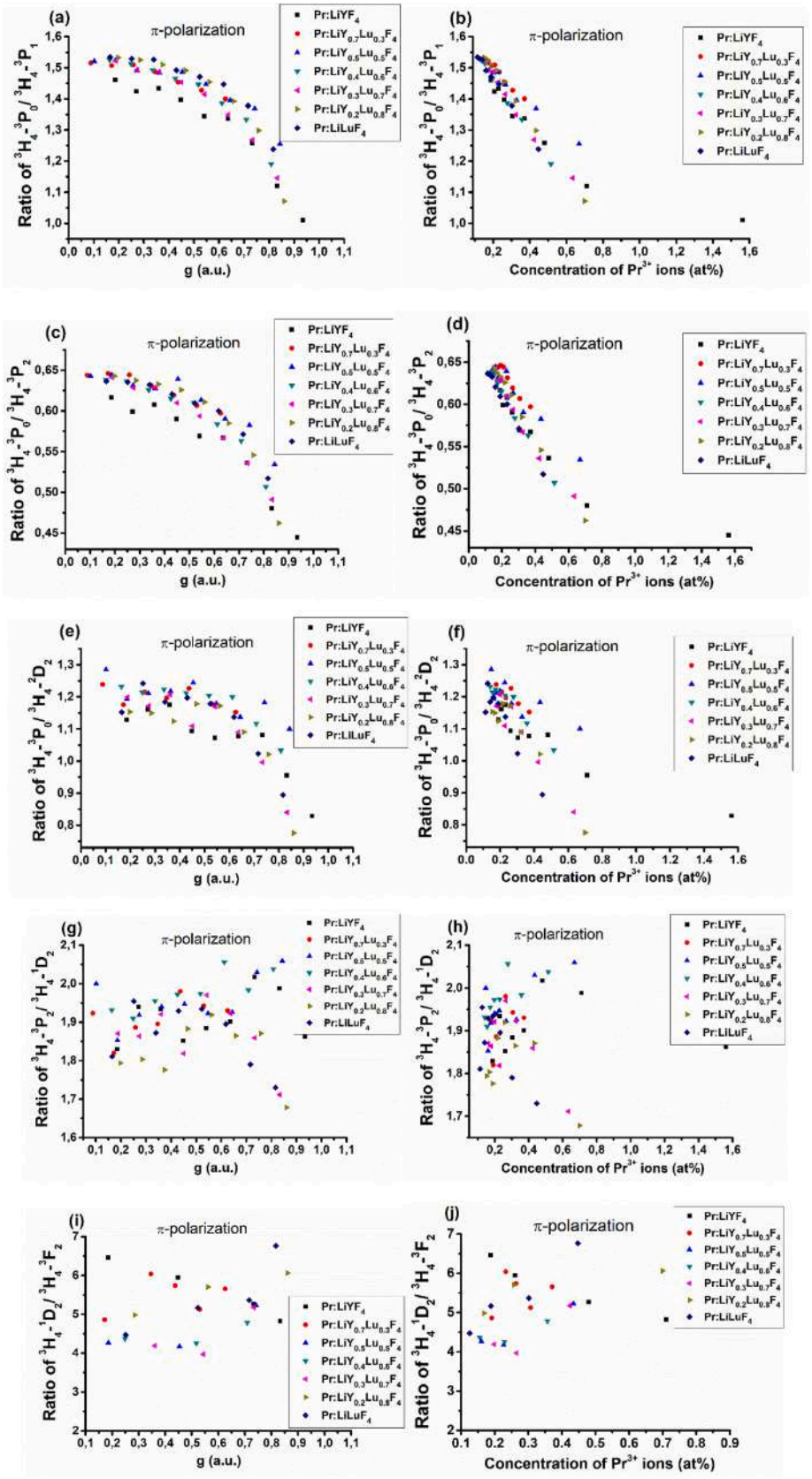

Fig. 5. Ratios of integral GSA absorption spectra for the transitions to different manifolds of Pr^{3+} ions in Pr:$LiY_{1-x}Lu_xF_4$ crystals versus the ingot crystallized part of the boules and the Pr^{3+} ions content.

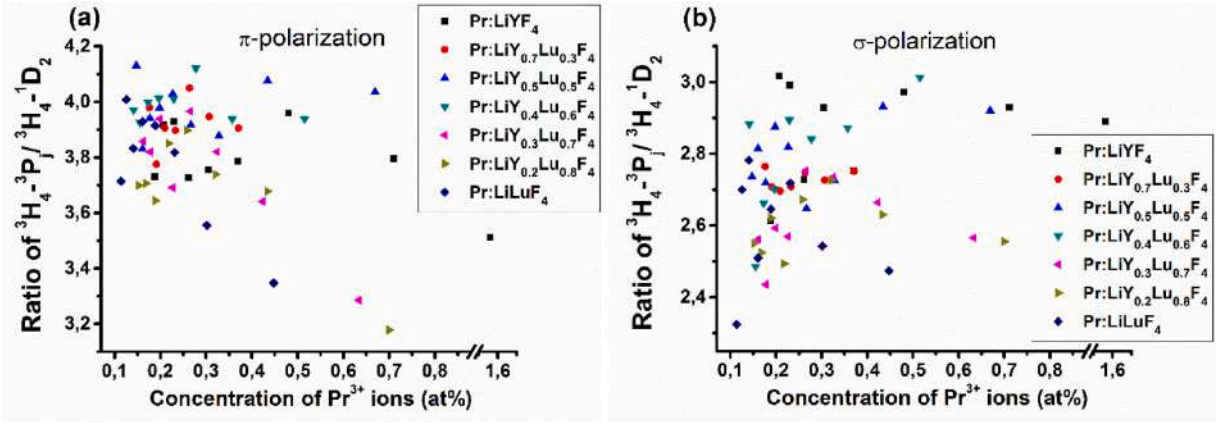

Fig. 6. Ratios of integral GSA polarized absorption spectra associated with $^3H_4$ - ^3P_j and $^3H_4$ -$^1D_2$ transitions of Pr^{3+} ions in Pr:$LiY_{1-x}Lu_xF_4$ crystals versus the dopant content.

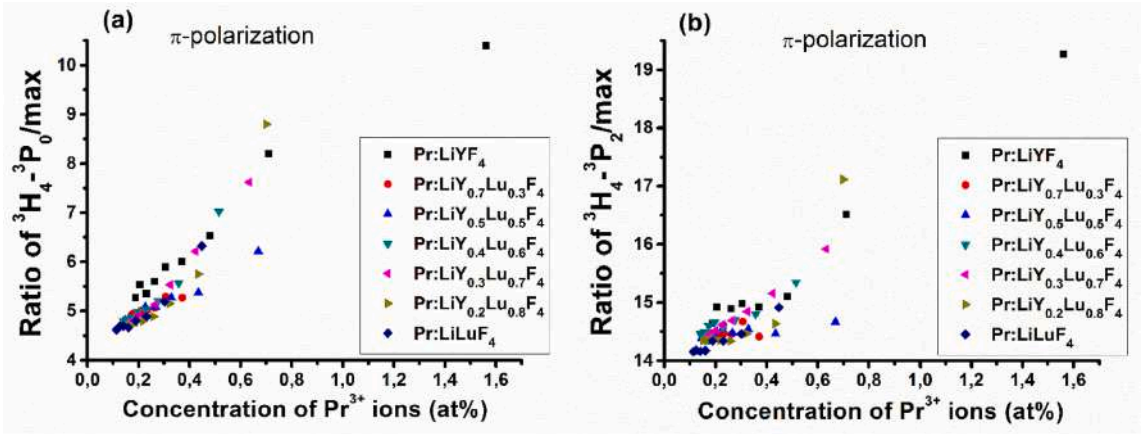

Fig. 7. Normalized to the maximal intensity integral GSA polarized absorption spectra associated with $^3H_4$ – $^3P_0$ and $^3H_4$ – $^3P_2$ transitions of Pr^{3+} ions in Pr:$LiY_{1-x}Lu_xF_4$ crystals versus the dopant content.

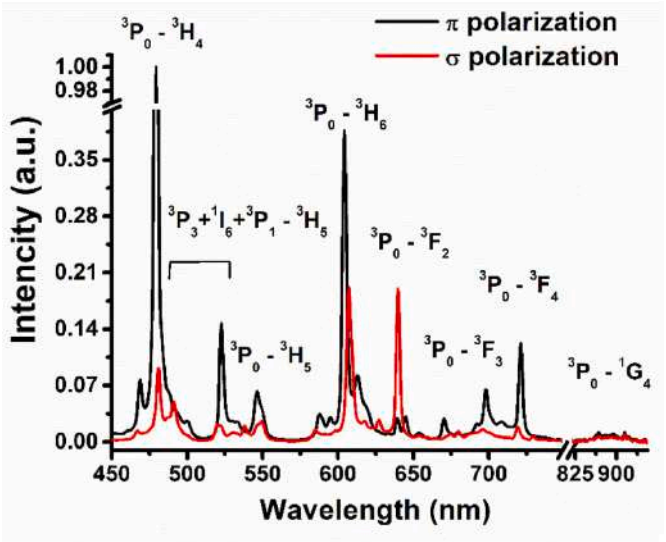

Fig. 8. Typical polarized spectra of Pr:$LiY_{1-x}Lu_xF_4$ crystals at the beginning of the growth.

observed is consistent to relative decreasing of $^3H_4 \rightarrow {}^3P_0$ absorption line intensity.

The luminescence decays from $^3P_0$ manifold of Pr^{3+} ions were studied. The typical fluorescence kinetics from the beginning, middle and end parts of the 1% Pr:$LiY_{1-x}Lu_xF_4$ crystals at room temperature are shown in Fig. 10.

The decay curves exhibit exponential behavior. The lifetime dependence for 1% Pr:$LiYF_4$, Pr:$LiY_{0.5}Lu_{0.5}F_4$, Pr:$LiLuF_4$ and 0.1% Pr:$LiY_{0.3}Lu_{0.7}F_4$ crystals as function of Pr^{3+} concentration is depicted on Fig. 11. The tendency of reducing of decay time is associated with concentration quenching of luminescence due to significant increasing of Pr^{3+} ions concentrations in the area of the end of bulk growth. The lifetime of $^3P_0$ state changes from about 47 μs for low-concentration parts to about 36 μs for high-concentration parts of the crystal boules. The results of approximation well coincide with 45.4 μs lifetime data for 0.19 at% Pr:$LiLuF_4$ sample [25], 38 μs for 0.45 at% Pr:$LiLuF_4$ and 36 μs for 0.65 at% Pr:$LiYF_4$ [10]. Based on Stark's structure data [33] we supposed that the cross-relaxation channel of losses is $^3P_0(^3P_1) - {}^1D_2 \rightarrow {}^3H_4 - {}^3H_6$ and is responsible for the concentration quenching.

The dependence of lifetime with the concentration of Pr^{3+} ions in $LiY_{1-x}Lu_xF_4$ can be used as a nondestructive method for determining the concentration in the sample.

3.3. Excited state absorption spectroscopy

The excited-state absorption measurements were carried out using

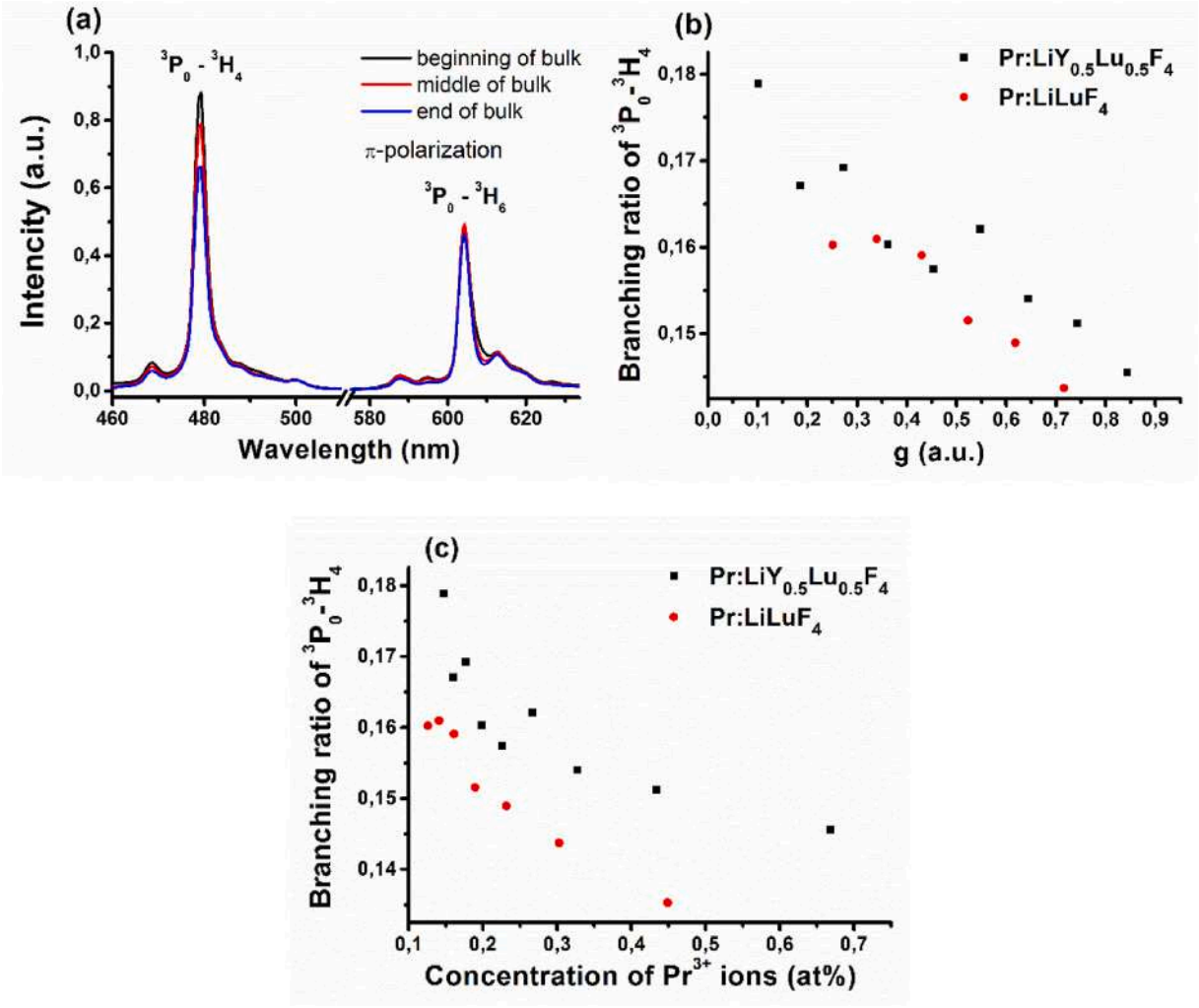

Fig. 9. The typical evolution of luminescence intensity of Pr:LiY$_{1-x}$Lu$_x$F$_4$ crystals along crystal growth direction (a) and branching ratios of Pr:LiY$_{0.5}$Lu$_{0.5}$F$_4$ and Pr:LiLuF$_4$ as a function of ingot crystallized part (b) and concentration of Pr^{3+} ions (c).

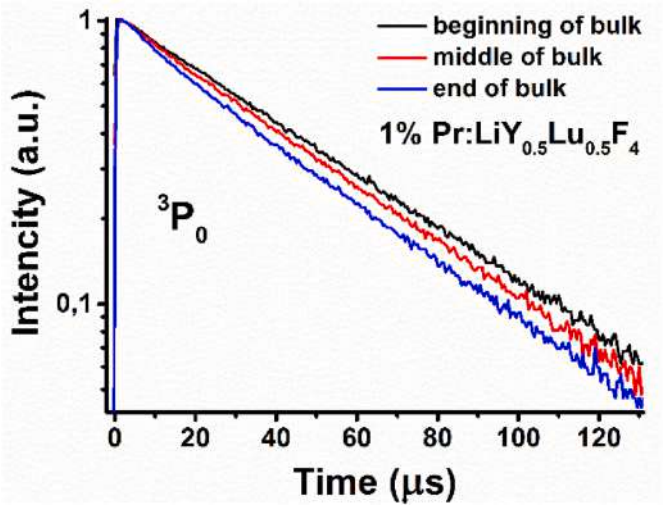

Fig. 10. The decays of luminescence from $^3P_0$ manifold of Pr^{3+} ions in Pr:LiY$_{0.5}$Lu$_{0.5}$F$_4$ crystal for beginning, middle and end parts of the bulk.

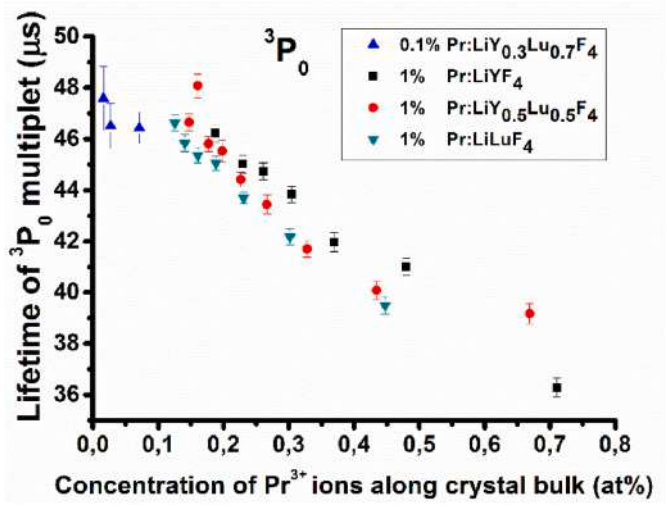

Fig. 11. Luminescence lifetimes of 0.1% Pr:LiY$_{0.3}$Lu$_{0.7}$F$_4$ and 1% Pr:LiYF$_4$, Pr:LiY$_{0.5}$Lu$_{0.5}$F$_4$, Pr:LiLuF$_4$ crystals as function of dopant concentration.

an optical parametric oscillator OPO pumped by the third harmonic of Nd:YAG laser as pump source. The pumping beam was π-polarized and its wavelength was tuned around 479 nm or 595 nm corresponding to the most intensive absorption bands of $^3H_4$ – $^3P_0$ or $^3H_4$ - $^1D_2$ transitions of Pr^{3+} ions, respectively. The pumping pulse energy was about 0.5–1.2 mJ with 3 ns (HWHM) pulse width. The laser operated at 10 Hz pulse repetition rate. The pumping beam was focused on the sample providing energy density per pulse between 0.25 and 0.6 J/cm^2.

The broadband emission from laser spark in xenon at high pressure induced by the fundamental harmonic of the same Nd:YAG laser was used as the probe. The pulse width of the probe beam was about 4.5 ns (FWHM) at pulse repetition rate 10 Hz and it was delayed by about 10 ns after pumping moment. The probe radiation was focused on the sample by fused silica lens and propagated through the sample in the opposite direction than the pumping beam. It was done to avoid the photodetector blinding by pumping radiation.

The spot of the probe beam was centered to the pump spot on the sample and had the diameter less than the pumping one. The probe radiation passed through the sample was collimated by the lens, analyzed by Glan-Taylor polarizer and focused to the waveguide of Stellarnet CCD spectrometer with spectral resolution 0.5 nm (Fig. 12). Measurements of pumping energy were realized by multichannel Ophir power meter.

To evaluate ESA cross-sections we excited $^1D_2$ and $^3P_0$ states of Pr^{3+} ions and estimated its population N by formula (1):

$$N = E\lambda/hcSd \quad (1)$$

where E – the absorbed pumping energy by the sample, λ – the pumping wavelength 479 nm or 595 nm, h – the Planck's constant, c – the speed of light S – the pumping area and d – the sample thickness. The absorbed energy E of pumping radiation was determined as the difference between the pumping energy incident to the sample and output one.

In the experiment we registered spectra intensities of the probe radiation passed through the unpumped $I_0(\lambda)$ and pumped $I(\lambda)$ sample. Spectrum $I(\lambda)$ contained the fluorescence spectrum $I_{lum}(\lambda)$ from the $^1D_2$ and ^3P_j states, that was also registered in the condition of probe beam absence and then subtracted form $I(\lambda)$ to calculate the sample transmittance $I_{tr}(\lambda)$:

$$I_{tr}(\lambda) = I_o(\lambda)/(I(\lambda) - I_{lum}(\lambda)) \quad (2)$$

Knowing excited states population N and transmittance spectrum $I_{tr}(\lambda)$ we estimated ESA cross-section spectra ($\sigma_{ESA}(\lambda)$) using Beer-Lambert law:

$$\sigma_{ESA}(\lambda) = \frac{1}{Nd} ln\left(I_o(\lambda)/(I(\lambda) - I_{lum}(\lambda))\right) \quad (3)$$

The ESA cross-section spectra are presented on Fig. 13 for π- and σ-polarizations of probing radiation.

The ESA cross-section values are in order of 10^{-18} cm^2 that is typical for $4f^n$-$4f^{n-1}5d$ parity-allowed electric-dipole transitions. All the ESA cross-sections of 1 at % Pr:$LiY_{1-x}Lu_xF_4$ crystals well coincide to each other. In contrast to absorption and luminescence caused by 4f-4f transitions we did not reveal any differences in ESA spectra registered along the crystal bulks. The detail analysis of obtained results manifested red shift of ESA peaks with «x» -parameter in chemical formula of $LiY_{1-x}Lu_xF_4$ samples that achieved 1 nm for Pr:$LiLuF_4$ compared to Pr:$LiYF_4$.

4. Conclusion

In the present search we presented the spatial-dependent behavior of 4f-4f and 4f-4f5d spectra of Pr:$LiY_{1-x}Lu_xF_4$ samples along crystal growth direction. The room temperature absorption, luminescence spectroscopic studies and kinetic measurements of Pr:$LiY_{1-x}Lu_xF_4$ crystals are performed. The GSA, luminescence and kinetic data revealed concentration-related broadening, changing of $^3H_4$ – ^3P_j spectra and reducing of lifetime of $^3P_0$ state of all the samples. The ESA cross-sections from ^3P_j and $^1D_2$ manifolds of Pr^{3+} ions were experimentally estimated. The ESA spectra do not demonstrate any concentration or spatial dependences. All the data are obviously critical important for further laser implementation in the visible region and the second harmonic generation.

CRediT authorship contribution statement

V.G. Gorieva: Investigation, Writing - original draft. **A.A. Lyapin:** Investigation. **P.A. Ryabochkina:** Resources, Conceptualization, Supervision, Conceptualization, Writing - review & editing. **V.V. Semashko:** Supervision, Conceptualization, Writing - review & editing.

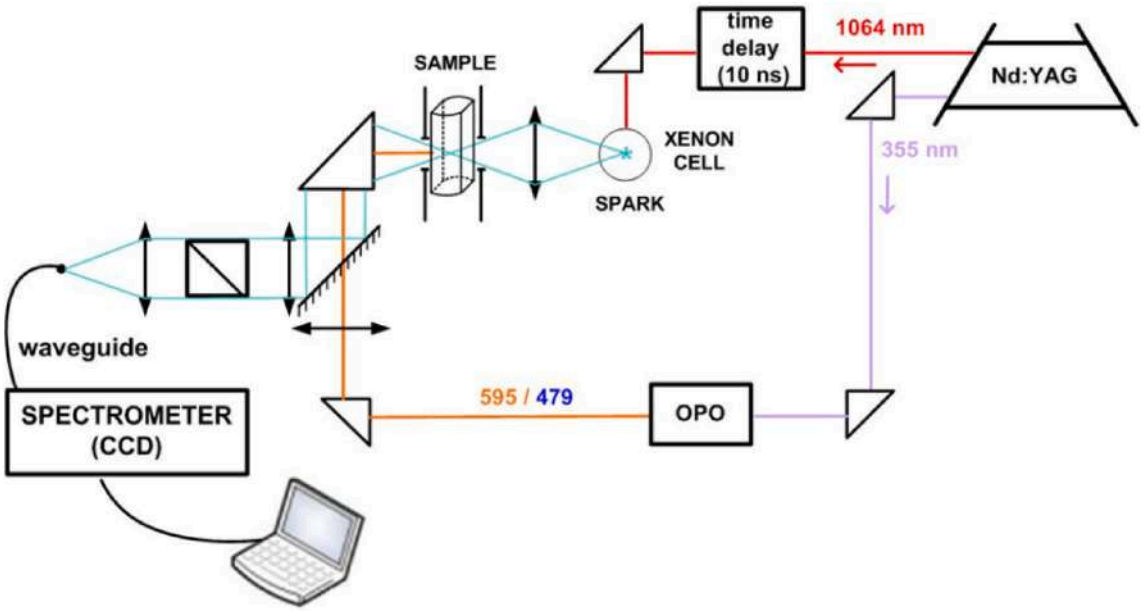

Fig. 12. The ESA experimental setup.

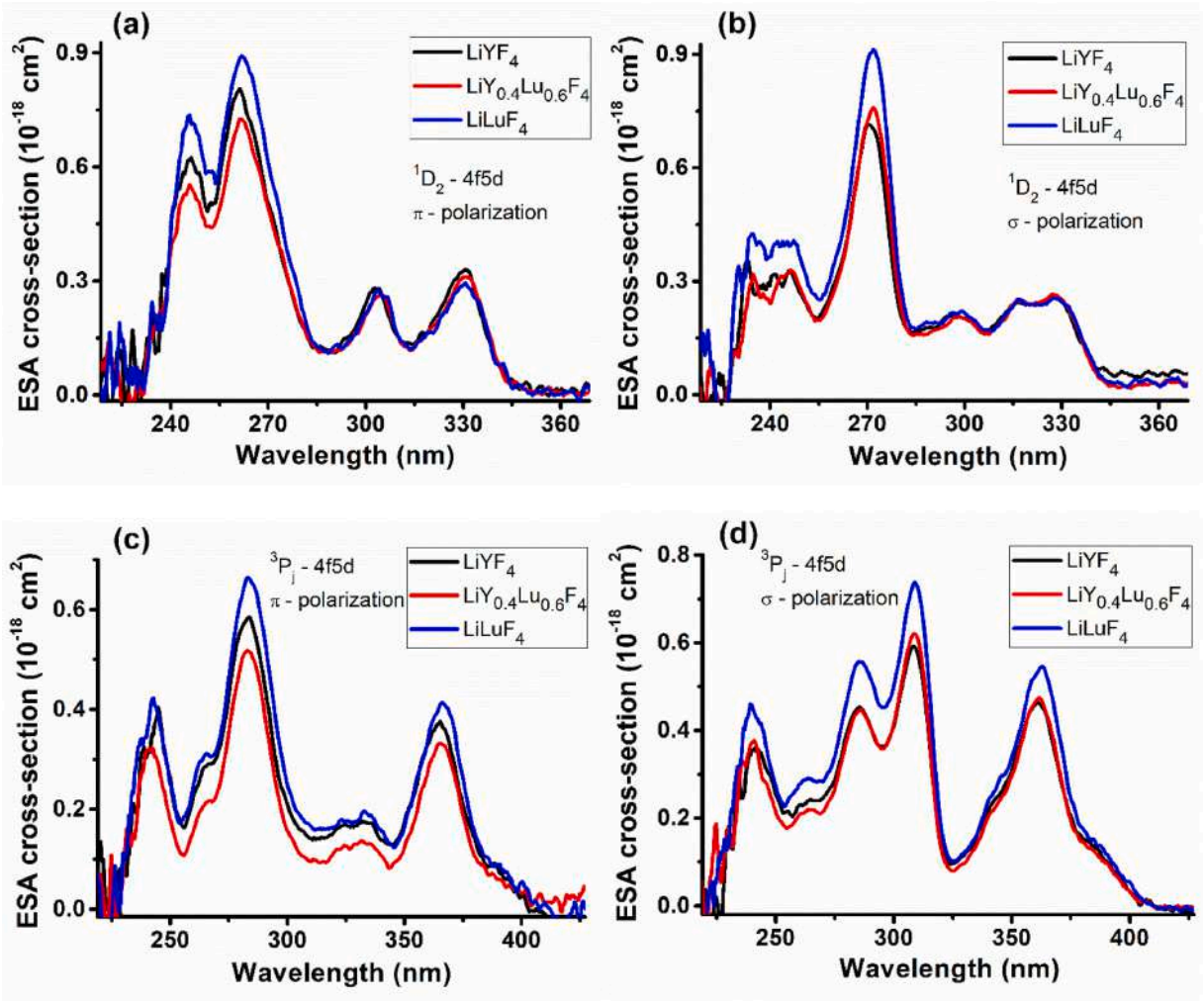

Fig. 13. Room temperature ESA cross-sections spectra of Pr^{3+}:$LiYF_4$, Pr^{3+}:$LiY_{0.4}Lu_{0.6}F_4$, and Pr^{3+}:$LiLuF_4$ single crystals from the $^1D_2$ (a,b), ^3P_j (c,d) manifolds of Pr^{3+} ions.

Acknowledgments

Luminescence and kinetics measurements were funded by the subsidy allocated to Kazan Federal University for the state assignment in the sphere of scientific activities (Project no. 3.1156.2017/4.6 and no. 3.5835.2017/6.7). Absorption spectroscopy experiments were supported by Russian Foundation for Basic Research (grant number 53/15-15) and were held in Mordovia State University. Modernization of the equipment for crystal growth and development of corresponding methods were performed under the framework and the financial support of the subsidy of the Russian Government (Agreement no. 02. A03.21.0002) to support the Program of Competitive Growth of Kazan Federal University among World's Leading Academic Centers. We are grateful to B.N. Kazakov for consultations in spectroscopic analysis.

References

[1] V.G. Gorieva, A.A. Lyapin, S.L. Korableva, B.N. Kazakov, V.V. Pavlov, V. M. Kyashkin, V.P. Mishkin, P.A. Ryabochkina, V.V. Semashko, Structural features and distribution coefficients of Pr^{3+}, Y^{3+} and Lu^{3+} ions in $LiY_{1-x}Lu_xF_4$ mixture crystals, J. Alloys Compd. 720 (2017) 1–7, https://doi.org/10.1016/j.jallcom.2017.04.327.

[2] N. Sugiyama, S. Fujita, Y. Hara, H. Tanaka, F. Kannari, Diode-pumped 640 nm Pr:YLF regenerative laser pulse amplifier, Optic Lett. 44 (2019) 3372, https://doi.org/10.1364/OL.44.003370.

[3] H. Okamoto, K. Kasuga, Y. Kubota, Efficient 521 nm all-fiber laser: splicing Pr^{3+}-doped ZBLAN fiber to end-coated silica fiber, Optic Lett. 36 (2011) 1470, https://doi.org/10.1364/OL.36.001470.

[4] A.S. Nizamutdinov, O.S. Morozov, S.L. Korableva, V.V. Semashko, E.B. Dunina, A. A. Kornienko, M.P. Demesh, N.V. Gusakova, A.S. Yasukevich, V.E. Kisel, N. V. Kuleshov, Cross sections, transition intensities, and laser generation at the $^3P_1 \rightarrow {}^3H_5$ transition of $LiY_{0.3}Lu_{0.7}F_4$:Pr^{3+} crystal, J. Appl. Spectrosc. 86 (2019) 220–225, https://doi.org/10.1007/s10812-019-00803-7.

[5] M. Olivier, J.-L. Doualan, P. Camy, H. Lhermite, P. Pirasteh, J.N. Coulon, A. Braud, J.-L. Adam, V. Nazabal, Optical amplification of Pr^{3+}-doped ZBLA channel waveguides for visible Laser emission, Optic Express 20 (2012) 25064, https://doi.org/10.1364/OE.20.025064.

[6] V. Ostroumov, W. Seelert, 522/261 nm cw generation of Pr:YLF laser pumped by OPS laser, Proc. SPIE 6451 (2007) 645104, https://doi.org/10.1117/12.705521.

[7] N. Niu, S. Pu, Q. Chen, Y. Wang, Y. Zhao, W. Wu, Q. Zheng, 302 nm continuous wave generation by intracavity frequency doubling of a diode-pumped Pr:YLF laser, Appl. Optic. 57 (2018) 9798–9802, https://doi.org/10.1364/AO.57.009798.

[8] P. Zhu, C. Zhang, K. Zhu, Y. Ping, P. Song, X. Sun, F. Wang, Y. Yao, 303 nm continuous wave ultraviolet laser generated by intracavity frequency-doubling of diode-pumped Pr^{3+}:$LiYF_4$ laser, Optic Laser. Technol. 100 (2018) 75–78, https://doi.org/10.1016/j.optlastec.2017.09.048.

[9] J.H. Li, X.H. Liu, J.B. Wu, X. Zhang, Y.L. Li, Diode pumped Pr^{3+}:$LiYF_4$-BBO ultraviolet laser at 320 nm, Laser Phys. 22 (2012) 523–526, https://doi.org/10.1134/S1054660X12030073.

[10] G. Huber, A. Richter, E. Heumann, Continuous wave Praseodymium solid-state lasers, Proc. SPIE 6451 (2007) 645102, https://doi.org/10.1117/12.708561.

[11] A. Richter, N. Pavel, E. Heumann, G. Huber, D. Parisi, A. Toncelli, M. Tonelli, A. Diening, W. Seelert, Continuous-wave ultraviolet generation at 320 nm by intracavity frequency doubling of red-emitting Praseodymium lasers, Optic Express 14 (2006) 3282–3287, https://doi.org/10.1364/OE.14.003282.

[12] Z. Liu, Z. Cai, B. Xu, C. Zeng, S. Huang, F. Wang, Y. Yan, H. Xu, Continuous-Wave ultraviolet generation at 349 nm by intracavity frequency doubling of a diode-pumped Pr:$LiYF_4$ laser, IEEE Photonics Journal 5 (2013) 1500905, https://doi.org/10.1109/JPHOT.2013.2271719.

[13] V. Ostroumov, W. Seelert, UV generation by intracavity frequency doubling of an OPS-pumped Pr:YLF laser with 500 mW of cw power at 360 nm, Proc. SPIE 6451 (2007) 645103, https://doi.org/10.1117/12.705526.

[14] X. Chen, Y. Shao, J.L. Yuan, D. Zhang, A.G. Wang, 303.5 nm cw Pr:BYF–BBO laser emission under 447 nm all-solid-state Nd:GdVO4–BiBO blue laser pumping, Laser Phys. Lett. 10 (2013), 065002, https://doi.org/10.1088/1612-2011/10/6/065002.

[15] Y. Dong, S.T. Li, X.H. Zhang, All-solid-state blue laser pumped Pr:KY_3F_{10}-BBO ultraviolet laser at 305 nm, Laser Phys. Lett. 9 (2012) 116–119, https://doi.org/10.1002/lapl.201110105.

[16] Y.L. Li, An efficient all-solid-state doubly resonant continuous-wave ultraviolet laser at 284 nm, Laser Phys. Lett. 10 (2013) 125006, https://doi.org/10.1088/1612-2011/10/12/125006.

[17] H. Jelınkov, M. Fibrich, M. Cech, K. Nejezchleb, V. Škoda, Blue generation of flash-lamp pumped Pr:YAP laser by intracavity frequency doubling, Laser Phys. Lett. 7 (2010) 34–37, https://doi.org/10.1002/lapl.200910110.

[18] M. Fibrich, J. Šulc, H. Jelínková, K. Nejezchleb, V. Škoda, Continuous-wave blue generation of intracavity frequency-doubled Pr:YAP laser, Optic Lett. 35 (2010) 214–216, https://doi.org/10.1364/OL.35.000214.

[19] S. Gianfaldoni, G. Tchernev, U. Wollina, M. Fioranelli, M.G. Roccia, R. Gianfaldoni, T. Lotti, An overview of laser in dermatology: the past, the present and the future (?), Open Access Maced. J. Med. Sci. 5 (2017) 526–530, https://doi.org/10.3889/oamjms.2017.130.

[20] V.I. Pauker, B.R. Thoma, G. Grass, P. Bleichert, M. Hanczaruk, L. Zöller, S. Zange, Improved discrimination of bacillus anthracis from closely related species in the bacillus cereus sensu lato group based on matrix-assisted laser desorption ionization–time of flight mass spectrometry, J. Clin. Microbiol. 56 (2018) e01900–e01917, https://doi.org/10.1128/JCM.01900-17.

[21] T. Briggs, G. Blunn, S. Hislop, R. Ramalhete, C. Bagley, D. McKenna, M. Coathup, Antimicrobial photodynamic therapy—a promising treatment for prosthetic joint infections, Laser Med. Sci. 33 (2018) 523–532, https://doi.org/10.1007/s10103-017-2394-4.

[22] M. Pudovkin, P. Zelenikhin, V. Shtyreva, O. Morozov, D. Koryakovtseva, V. Pavlov, Y. Osin, V. Evtugyn, A. Akhmadeev, A. Nizamutdinov, V. Semashko, Coprecipitation method of synthesis, characterization, and cytotoxicity of Pr^{3+}: LaF3 (CPr = 3, 7, 12, 20, 30%) nanoparticles, J. Nanotechnology (2018) 8516498, https://doi.org/10.1155/2018/8516498.

[23] B. Bishop, Y. Geffen, A. Plaut, O. Kassis, R. Bitterman, M. Paul, A. Neuberger, The use of matrix-assisted laser desorption/ionization time-of-flight mass spectrometry for rapid bacterial identification in patients with smear-positive bacterial meningitis, Clin. Microbiol. Infect. 24 (2018) 171–174, https://doi.org/10.1016/j.cmi.2017.05.014.

[24] A. Richter, E. Heuman, G. Huber, V. Ostroumov, W. Seelert, Power scaling of semiconductor laser pumped Praseodymium lasers, Optic Express 15 (2007) 5172–5178, https://doi.org/10.1364/OE.15.005172.

[25] F. Cornacchia, A. Richter, E. Heumann, G. Huber, D. Parisi, M. Tonelli, Visible laser emission of solid state pumped $LiLuF_4$:Pr^{3+}, Optic Express 15 (2007) 992–1002, https://doi.org/10.1364/OE.15.000992.

[26] I.M. Ranieri, S.P. Morato, L.C. Courrol, H.M. Shihomatsu, A.H.A. Bressiani, N.M. P. Moraes, Growth of $LiY_{(1-x-y)}Lu_xN_yF_4$ crystals for optical applications, J. Cryst. Growth 209 (2000) 906–910, https://doi.org/10.1016/S0022-0248(00)00473-5.

[27] Y. Yokota, A. Yamaji, T. Yanagida, N. Kawaguchi, K. Fukuda, A. Yoshikawa, The control of mean ionic radius at Y site by Lu co-doping for Ce:$LiYF_4$ single crystals, J. Cryst. Growth 362 (2013) 243–246, https://doi.org/10.1016/j.jcrysgro.2011.11.020.

[28] A.S. Nizamutdinov, V.V. Semashko, A.K. Naumov, S.L. Korableva, R. Yu Abdulsabirov, A.N. Polivin, M.A. Marisov, Optical and gain properties of series of crystals LiF–YF_3–LuF_3 doped with Ce^{3+} and Yb^{3+} ions, J. Lumin. 127 (2007) 71–75, https://doi.org/10.1016/j.jlumin.2007.02.011.

[29] D.S. Knowles, Z. Zhang, D. Gabbe, H.P. Jenssen, Laser action of Pr^{3+} in $LiYF_4$ and spectroscopy of Eu^{3+}-sensitized Pr in BaY_2F_8, J. Quant. Econ. 24 (1988) 1118–1123, https://doi.org/10.1109/3.235.

[30] Z. Liu, Z. Cai, S. Huang, C. Zeng, Z. Meng, Y. Bu, Z. Luo, B. Xu, H. Xu, C. Ye, F. Stareki, P. Camy, R. Moncorgé, Diode-pumped Pr^{3+}:$LiYF_4$ continuous-wave deep red laser at 698 nm, Opt. Soc. Amer. B. 30 (2013) 302–305, https://doi.org/10.1364/JOSAB.30.000302.

[31] A. Sottile, Z. Zhang, S. Veronesi, D. Parisi, A. Di Lieto, M. Tonelli, Visible laser operation in a Pr^{3+}:$LiLuF_4$ monocrystalline fiber grown by the micro-pulling-down method, Opt. Mater. Express 6 (2016) 1964–1972, https://doi.org/10.1364/OME.6.001964.

[32] B. Xu, Z. Liu, H. Xua, Z. Cai, C. Zeng, S. Huang, Y. Yana, F. Wang, P. Camy, J. L. Doualan, A. Braud, R. Moncorgé, Highly efficient InGaN-LD-pumped bulk Pr:YLF orange laser at 607nm, Optic Commun. 305 (2013) 96–99, https://doi.org/10.1016/j.optcom.2013.05.002.

[33] S. Nicolas, E. Descroix, Y. Guyot, M.-F. Joubert, R. Yu Abdulsabirov, S. L. Korableva, A.K. Naumov, V.V. Semashko, 4f2 to 4f5d excited state absorption in Pr^{3+}-doped crystals, J. Opt. Mat. 16 (2001) 233–242, https://doi.org/10.1016/S0925-3467(00)00083-5.

[34] B. Xu, P. Camy, J.L. Doualan, Z.P. Cai, R. Moncorge, Visible laser operation of Pr^{3+}-doped fluoride crystals pumped by a 469 nm blue laser, Optic Express 19 (2011) 1191–1197, https://doi.org/10.1364/OE.19.001191.

[35] S. Khiari, M. Velazquez, R. Moncorge, J.L. Doualan, P. Camy, A. Ferrier, M. Diaf, Red-luminescence analysis of Pr^{3+} doped fluoride crystals, J. Alloys Compd. 451 (2008) 128–131, https://doi.org/10.1016/j.jallcom.2007.04.233.

[36] E. Damiano, J. Shu, A. Sottile, M. Tonelli, Spectroscopy and visible laser operations of a μ-PD grown Pr3+ LiYF, J. Phys. D Appl. Phys. 50 (2017) 135107, https://doi.org/10.1088/1361-6463/aa5f4b.

[37] A. Lyapin, V. Gorieva, S. Korableva, S. Artemov, P. Ryabochkina, V. Semashko, Diode-pumped $LiY_{0.3}Lu_{0.7}F_4$:Pr and $LiYF_4$:Pr red lasers, Laser Phys. Lett. 13 (2016) 125801, https://doi.org/10.1088/1612-2011/13/12/125801.

[38] F. Starecki, Épitaxie de $LiYF_4$ dopé Pr pour laser en guide d'onde, Université de Caen, France, 2013.

[39] V. Tikhomirov, S. Tikhomirova, Hypersensitive transition $^3P_0$-$^3F_2$ of Pr^{3+} related to the polarizability and structure of glass host, J. Non-Cryst. Solids 274 (2000) 50–54, https://doi.org/10.1016/S0022-3093(00)00202-7.

[40] Oscar L. Malta, F. de Sa Gilberto, Explanation of the anomalous hypersensitive $^3H_4$-$^3P_2$ transition in Pr^{3+}, J. Physical Review Letters 45 (1980) 890–893, https://doi.org/10.1103/PhysRevLett.45.890.

[41] M. Stef, I. Nicoară, D. Vizman, Distribution of Yb^{3+} and Yb^{2+} ions along YbF_3-doped BaF_2 crystals, Cryst. Res. Technol. (2018) 1800186, https://doi.org/10.1002/crat.201800186.

[42] D.E. McCumber, Einstein relations connecting broadband emission and absorption spectra, J. Physical Review 136 (1964) 954–957, https://doi.org/10.1103/PhysRev.136.A954.